INSTITUTE OF PHYSICS PUBLISHING PHYSICS IN MEDICINE AND BIOLOGY

Phys. Med. Biol. **46** (2001) 1343–1355 www.iop.org/Journals/pb PII: S0031-9155(01)20109-2

Importance of the choice of the collimator for the detection of small lesions in scintimammography: a phantom study

Irène Buvat[1], Sophie Laffont[2], Joseph Le Cloirec[2], Patrick Bourguet[2] and Robert Di Paola[1]

[1] U494 INSERM, CHU Pitié-Salpêtrière, 91 Boulevard de l'Hôpital, 75 634 Paris Cedex 13, France
[2] Service de Médecine Nucléaire, Centre Régional de Lutte contre le Cancer Eugène Marquis, Rue de la Bataille des Flandres, BP 6279, 35 062 Rennes Cedex, France

E-mail: buvat@imed.jussieu.fr

Received 15 December 2000

Abstract

^{99m}Tc methoxyisobutylisonitrile planar scintimammography (SMM) is mostly performed using low-energy high-resolution (LEHR) parallel collimators. We studied whether using a different collimator could improve the detection of small (<1.5 cm) lesions for which SMM sensitivity is poor. Thirty four breast phantom configurations were considered, either with hot spheres simulating lesions or without any spheres. For each configuration, four planar acquisitions were performed using LEHR, low-energy ultra high-resolution (LEUHR), high-resolution fan-beam (HRFB) and ultra high-resolution fan-beam (UHRFB) collimators. Images corresponding to the 20% and 10% energy windows and to the Jaszczak subtraction were calculated. A database including 156 borderline images was derived. After training, 10 observers scored the images for the presence of a sphere. The performances in sphere detection were studied using receiver operating characteristic (ROC) analysis. For all types of image, the area under the ROC curve was highest with the UHRFB collimator and lowest with either the LEUHR or the HRFB collimator. For the 10% energy window images conventionally used in SMM, the detection sensitivities averaged 91%, 73%, 60% and 55% for the UHRFB, LEHR, HRFB and LEUHR collimators respectively, for the same specificity of 64%. We conclude that detection of small tumours in planar SMM might be significantly improved by using a UHRFB collimator instead of an LEHR collimator.

(Some figures in this article are in colour only in the electronic version; see `www.iop.org`)

1. Introduction

Scintimammography (SMM) can be a useful adjunct to physical examination and mammography for the detection and characterization of breast tumours, especially for patients

with dense breast tissue, architectural distortion of the breast, breast implant or with equivocal mammography (Taillefer 1999). However, one major limitation of SMM is its poor sensitivity for detecting non palpable lesions which are typically less than 1 cm in diameter (e.g. Mekhmandarov *et al* 1998, Scopinaro *et al* 1998). The detection of lesions measuring less than 5 to 7 mm in diameter has not been reported to date. To improve the value of SMM, various technical aspects have been carefully studied, such as the dose of radiotracer, the position of the patient (prone versus supine) (Khalkhali *et al* 1994), the time between the injection and the scan, the use of conventional (non-dedicated) SPECT instead of planar imaging (Palmedo *et al* 1996) or even the effect of scatter correction (Buvat *et al* 1998). As the spatial resolution of conventional gamma cameras is mainly responsible for the poor sensitivity of SMM in detecting small lesions, dedicated cameras are currently being developed and assessed (e.g. Maini *et al* 1999, Scopinaro *et al* 1999). Before these new detectors are available for widespread use, another way to improve the spatial resolution of conventional gamma cameras could be to use a higher resolution collimator. Most SMM scans are currently performed using a low-energy high-resolution (LEHR) collimator, which is the collimator recommended in the SMM procedure guideline (Khalkhali *et al* 1999). The purpose of this study was to determine whether using a different collimator could significantly increase the sensitivity of lesion detection in SMM.

2. Materials and methods

2.1. Phantom

As it was not possible to scan the same patients twice with different collimators, the performance of different collimators for lesion detection was studied using an anthropomorphic breast phantom (ECT/FL-BR/A, figure 1) from Data Spectrum Corporation, Hillsborough, NC. This phantom consists of two vacuum-formed plastic breasts (900 and 1000 ml in volume respectively) mounted on an acrylic base (model ECT/RING-3/A) simulating the thoracic surface that can be fixed to an elliptical cylinder (model ECT/ELP/P) to simulate the thorax. The thoracic compartment can itself include a heart compartment. Small spheres can be inserted in the breast at different depths to simulate tumours. Spheres that were 9.8, 12.4 and 15.8 mm in diameter (sphere volumes of 0.5, 1 and 2 ml) were placed at two different depths in the phantom: 70 and 95 mm. The spheres were filled with a ^{99m}Tc solution with sphere-to-background activity ratios equal to 2, 3, 4 or 6 and breast background activity varying from 37 to 400 MBq in the 900 ml breast. No activity was introduced in the thorax or in the heart cavity. In addition, acquisitions without any spheres were performed with activity varying from 30 to 777 MBq in the breast.

2.2. Acquisitions

All acquisitions were performed on a DST-XL gamma camera (SMVi, Buc, France) with an intrinsic spatial resolution equal to 3.7 mm.

2.2.1. Collimator characteristics. The acquisitions were performed using four collimators with different characteristics (table 1): a low-energy high-resolution (LEHR) collimator, a low-energy ultra high-resolution (LEUHR) collimator, a high-resolution fan-beam (HRFB) collimator and an ultra high-resolution fan-beam (UHRFB) collimator. The images were acquired using a 256 $\times$ 256 matrix, with a zoom of 2, giving a pixel size of 1.13 mm $\times$ $1.13/G$ mm where G was the magnification factor ($G = 1$ for the LEHR and LEUHR

Figure 1. Breast phantom.
(This figure is in colour only in the electronic version, see `www.iop.org`)

Table 1. Physical characteristics of the four collimators.

Collimator	Flat-side to flat-side hole dimension (mm)	Hole length (mm)	Septal thickness (mm)	Focal length (mm)
LEHR	3	65	0.25	—
LEUHR	1.9	47	0.2	—
HRFB	2.3	47	0.23	552.6
UHRFB	1.9	50	0.23	548.6

collimators, and G different from 1 for the HRFB and UHRFB collimators). The collimator characteristics were used to calculate the theoretical sensitivity and spatial resolution (characterized by the full width at half maximum (FWHM)) of the imaging system equipped with each collimator (Moore *et al* 1992). We also calculated an additional quality index, called signal density, by dividing the sensitivity value by the magnification factor G of the collimator. This index was proportional to the mean number of counts per pixel for a given activity (since the pixel size was $1.13 \times 1.13/G$). As the noise is Poisson in planar scintigraphic images, the variance of the noise in a pixel is equal to the number of counts in that pixel, and the signal density index was therefore inversely related to the noise level in the image.

On the other hand, the spatial resolution, sensitivity and signal density for the gamma camera equipped with each collimator were experimentally determined. To measure the spatial resolution, a 20% (126–154 keV) image of a line source (1.2 mm in diameter) of 296 MBq of ^{99m}Tc was acquired at 7 cm and 10 cm from the collimator. To measure the sensitivity of the imaging system, a 10 cm diameter Petri dish filled with 74 MBq of ^{99m}Tc was used. The sensitivity was measured for dish to collimator distances of 7 cm and 10 cm respectively. The signal density was calculated by drawing a region of interest (ROI) around the Petri dish, and dividing the total number of counts in that ROI by the number of pixels included in the ROI.

2.2.2. Phantom acquisitions. Fourteen configurations with a sphere were studied, the characteristics of which are listed in table 2 in terms of the size of the sphere, its depth and the sphere-to-background activity ratio. For each configuration, four planar acquisitions,

each lasting 10 min, were performed, one with each collimator.

Table 2. Characteristics of the phantom configurations when a sphere was introduced in the breast. Configurations included in the borderline image base are shown in bold print.

Configuration number	Sphere diameter (mm)	Sphere depth (mm)	Sphere-to-background activity ratio
1	**9.8**	**70**	**3**
2	**9.8**	**70**	**4**
3	9.8	70	6
4	**9.8**	**95**	**2**
5	**9.8**	**95**	**3**
6	**12.4**	**70**	**2**
7	**12.4**	**70**	**3**
8	12.4	70	4
9	12.4	70	6
10	**12.4**	**95**	**2**
11	**12.4**	**95**	**3**
12	15.8	70	3
13	15.8	70	4
14	15.8	70	6

In addition, 20 planar acquisitions (each lasting 10 min) of the breast without any spheres were performed, corresponding to five acquisitions (activity in the breast varying from 30 MBq and 777 MBq) with each of the four collimators.

For each acquisition, the collimator was in contact with the surface of the breast, corresponding to a prone lateral imaging situation. Three types of image were obtained: the image I20 corresponding to the 20% energy window (126–154 keV), the image I10 corresponding to the 10% energy window (133–147 keV) and the image I_{JAS} resulting from the Jaszczak subtraction (Jaszczak *et al* 1985). The latter was calculated by subtracting the image acquired in a Compton energy window (92–125 keV) $I_{compton}$ from the I20 image using

$$I_{JAS} = I20 - 0.5 \times I_{compton}. \quad (1)$$

In total, 228 images were obtained, namely 168 including a sphere (14 configurations $\times$ four collimators $\times$ three types of image) and 60 without a sphere (20 acquisitions $\times$ three types of image).

2.3. Creation of an image base

The 56 I20 images corresponding to acquisitions of the phantom with a sphere were carefully reviewed in random order by an observer unaware of the configuration parameters and of the collimator used. For each configuration, the four images corresponding to the four collimators were included in the final image base only if the sphere was considered to be 'difficult to detect' in at least one of the four images. This selection process resulted in 96 images containing a sphere (eight configurations shown in bold in table 2 $\times$ four collimators $\times$ three types of image). These 96 images together with the 60 images without spheres yielded an image base of 156 images, in which the images were randomly ordered.

In addition, eight borderline images from additional acquisitions were selected (four with a sphere and four without), to serve as a learning image base. In this image base, there were two images for each collimator (one with a sphere and one without), four images I20, two images I10 and two images I_{JAS}.

2.4. Image reading

Ten observers from two institutions (U494 INSERM, Paris and the Department of Nuclear Medicine, Rennes) were asked to read the image base, after a training session using the learning image base. All observers (five nuclear physicians and five medical physicists working in a nuclear medicine department) were experienced in nuclear medicine image reading, although not all of them had the same level of experience and not all of them were used to SMM images. The images were read directly on the computer screen, using either the rainbow type colour scale (U494 INSERM) or the grey colour scale (Rennes) the observers were used to. The observers were free to adjust the brightness and contrast as they wished. For each image, the observer was asked to give a score between 1 and 5 (1, sphere certainly absent; 2, sphere probably absent; 3, undetermined; 4, sphere probably present; 5, sphere certainly present). No information was given regarding the proportion of images containing a sphere in the image base. The results of the readings were analysed to derive receiver operating characteristic (ROC) curves (Metz 1986).

2.5. Data analysis

For each observer, the 156 scores were sorted into 12 groups of 13 scores, each group corresponding to a pair of collimator (LEHR, LEUHR, HRFB or UHRFB) and type of image (I20, I10 or I_{JAS}). For each group, an ROC curve (Metz 1986) was calculated and the reading performances were characterized using the area under that ROC curve (AUC) calculated using the trapezoidal rule and the corresponding standard error (Hanley and McNeil 1982). This resulted in 120 ROC curves and associated AUC.

To test whether the impact of the collimator upon sphere detection depended on the type of image (I20, I10 or I_{JAS}), each set of 40 AUC (10 observers $\times$ four collimators) corresponding to each type of image was independently analysed using a Friedman two-way analysis of variance by ranks (Siegel and Castellan 1988). For each image type, the null hypothesis was that the four samples of 10 AUC values (corresponding to the four collimators) were drawn from the same population. Results were considered to be statistically significant for $p < 0.05$. When the null hypothesis was rejected, multiple comparisons between the four collimators were performed using the Wilcoxon signed ranks test (Siegel and Castellan 1988) to find where the differences were. A Bonferroni correction was used to account for multiple comparisons, hence $p < 0.008$ was considered to be a significant difference with a 95% confidence.

3. Results

3.1. Collimator characteristics

For each collimator, the theoretical (Moore *et al* 1992) and experimental values of spatial resolution, sensitivity and signal density are given in table 3, for two distances between the object and the collimator (7 and 9.5 cm for the theoretical calculations, and 7 and 10 cm for the experimental measurements).

As expected, the ultra high-resolution collimators had a better spatial resolution than the corresponding high-resolution collimators, together with a poorer sensitivity, for the distances that were considered. The best spatial resolution was obtained with the UHRFB collimator, while the poorest was observed with the LEHR collimator. The best sensitivity was obtained with the HRFB collimator while the LEUHR collimator presented the poorest sensitivity. The highest signal density (corresponding to the lowest level of noise per pixel) was observed with the LEHR collimator.

Table 3. Experimental and theoretical (in parentheses) values of spatial resolution, sensitivity and signal density for each collimator.

	Spatial resolution (mm)		Collimator sensitivity (arbitrary units)		Signal density (arbitrary units)	
Collimator	7 cm	10 (9.5) cm	7 cm	10 (9.5) cm	7 cm	10 (9.5) cm
LEHR	7.2 (7.5)	8.4 (8.5)	188 (49)	188 (49)	88 (49)	88 (49)
LEUHR	6.2 (6.2)	7 (7)	139 (36)	139 (36)	66 (36)	66 (36)
HRFB	6.5 (6.4)	7.6 (7.4)	229 (69)	241 (73)	80 (48)	78 (45)
UHRFB	5.5 (5.4)	5.8 (6.1)	148 (40)	157 (43)	49 (25)	49 (23)

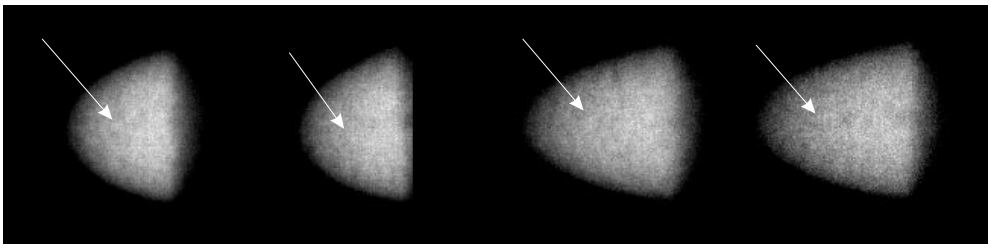

Figure 2. Examples of borderline images included in the image base. The breast included a 70 mm deep sphere (12.4 mm in diameter) with a sphere-to-background activity ratio of 2. From left to right, the images correspond to the 20% (I20) image acquired with the four different collimators. The location of the sphere is indicated by the white arrows.

3.2. Borderline images

The selection of borderline images indicated that spheres that were 15.8 mm in diameter could always be easily detected in our phantom, while spheres that were 12.4 or 9.8 mm in diameter were harder to detect, especially those with a low sphere-to-background ratio (from 2 to 4) (configurations shown in bold print in table 2). Spheres with a diameter of 9.8 mm and a sphere-to-background ratio of 6 at a depth of 7 cm in the breast could be easily detected but spheres that were 12.4 mm in diameter but which were deep in the breast could not easily be seen. Examples of I20 images obtained with the four collimators for the 12.4 mm sphere at a depth of 70 mm with a sphere-to-background activity ratio of 2 are shown in figure 2.

3.3. ROC results

The AUC resulting from the ROC analyses for each observer and each collimator are reported in tables 4, 5 and 6 for image types I20, I10 and I_{JAS} respectively.

For all image types (I20, I10 and I_{JAS}), the detection performances, as measured by the AUC, varied substantially between observers, but some trends were observed. The highest AUC was obtained with the UHRFB collimator for 6 out of 10 observers in the I20 images, for 9 out of 10 observers in the I10 images and for 5 out of 10 observers in the I_{JAS} images, while the highest AUC was observed with the LEHR collimator for only 3 out of 10 observers in the I20 and I_{JAS} images and for none of the observers in the I10 images. The HRFB collimator yielded the highest AUC only for one observer with the I20 and I10 images and for two observers with the I_{JAS} images, while the LEUHR collimator never yielded the highest AUC. Averaging the AUC values over the 10 observers (last row of tables 4, 5 and 6), the highest

mean AUC was obtained with the UHRFB collimator, followed by the LEHR collimator, for all types of image (I20, I10 and I_{JAS}). The poorest sphere detection was obtained either with the LEUHR collimator or with the HRFB collimator. For each type of image, the Friedman two-way analysis of variance showed that the null hypothesis according to which the four sets of AUC values corresponding to the four collimators were drawn from the same population was rejected at a 0.01 level of significance. To find out where the differences were, multiple comparisons between the four collimators were performed (table 7) which showed that for the three image types, the UHRFB collimator yielded significantly better detection performances than the HRFB or LEUHR collimator. In addition, for the I10 images, the UHRFB collimator also yielded better performance than the LEHR collimator. Finally, the LEHR collimator yielded better detection than the LEUHR and HRFB collimators for the I_{JAS} images.

To determine how the differences in AUC translated into differences in sensitivity/specificity trade-off, for each observer, each collimator and each image type, the sensitivity leading to a specificity value as close to 60% as possible was determined and the corresponding sensitivity/specificity trade-off was considered. Sensitivity values could then be compared for a specificity of around 60%. The resulting sensitivity and specificity values averaged over the 10 observers are given in table 8. This table shows that for all image types the UHRFB collimator yielded a better sensitivity/specificity trade-off than the LEHR collimator. For instance, for the I10 images, which are conventionally used in SMM, the sensitivity was 91% with the UHRFB collimator against 72.5% with the LEHR collimator, for a same specificity of 64% ($p < 0.05$, t-test). The sensitivity was also higher with the UHRFB collimator than with the LEHR collimator for the I20 and I_{JAS} images, although these differences were not significant. For all image types, the sensitivity/specificity trade-off was the poorest with the LEUHR and HRFB collimators, with a sensitivity about 10% lower than that observed with the LEHR collimator and more than 15% lower than that observed with the UHRFB collimator.

4. Discussion

4.1. Rationale

The main weakness of conventional SMM lies in its poor sensitivity for lesions less than 1.5 cm in diameter. Although SPECT imaging could be a good candidate for better detection of small lesions, it cannot be recommended for SMM yet (Khalkhali *et al* 1999), because it makes it more difficult to locate the lesion and tends to decrease the specificity of lesion detection. In planar imaging, current guidelines for performing SMM recommend the use of an LEHR collimator (Khalkhali *et al* 1999). Since the ability to detect small lesions depends on spatial resolution, which is mostly a function of the collimator characteristics, using a collimator different from the LEHR could improve lesion detection. The feasibility of dedicated breast SPECT with a pinhole collimator mounted on a conventional SPECT camera has already been shown by Scarfone *et al* (1997): two spheres that were 6.4 and 9.6 mm in diameter with sphere-to-background activity ratios of 7.7 and 5 respectively could be more easily seen on the pinhole SPECT images than in the planar pinhole or LEUHR images, but no visual benefit of using planar pinhole imaging instead of planar LEUHR imaging was reported. No comparison was made with the LEHR collimator in this study. The potential of pinhole collimation compared with parallel collimation has also been demonstrated in planar imaging using visual inspection of sample images (Tsui *et al* 1998).

4.2. Determination of borderline cases

To determine whether changing any component in the imaging protocol can improve the detection of lesions, it is necessary to focus on cases in which the lesions are difficult to detect. For the Data Spectrum breast phantom with breast activity only, borderline cases were obtained with a sphere that was 12.4 mm in diameter (1 ml) or less, located at a depth of 70 or 95 mm, and a sphere-to-background activity ratio of 2 or 3. The smallest sphere (0.5 ml, 9.8 mm in diameter) could not be seen at a depth of 70 mm for a sphere-to-background activity ratio of 4. These sphere-to-background activity ratios are realistic, since measurements from excised tissues revealed tumour-to-background concentration ratios of between 1.4 and 5.7 in patients (Maublant *et al* 1996). In the presence of thoracic and cardiac activity, the borderline cases as defined in this study are expected to remain borderline, but larger spheres, spheres presenting a higher sphere-to-background ratio or more superficial spheres might also yield borderline images.

4.3. ROC analysis

To study whether our results would differ depending on the type of image (I20, I10 or I_{JAS}), the impact of the collimator has been independently studied for these three types of image using ROC analyses. As a result, the number of images of one type (I20, I10 or I_{JAS}) obtained with one collimator was low (13 images). ROC analysis was performed using a non-parametric approach (no distributional assumptions): the AUC values were calculated using the trapezoidal rule, which is equivalent to the Wilcoxon statistic or to the probability of a correct ranking of a (without a sphere, with a sphere) pair and the associated standard errors were obtained from the variance of the Wilcoxon statistic (Hanley and McNeil 1982). Although this approach systematically underestimates the AUC that would be obtained using a maximum likelihood parametric technique (Dorfman and Alf 1969), it guards against the possibility of incorrect distributional assumptions. To counteract the low statistical power due to the low number of images used for each ROC analysis, the consistency of the results obtained from 10 observers was studied to test statistical significance.

4.4. Impact of the collimator

For borderline cases, the AUC values showed that for any type of image (I20, I10 or I_{JAS}), using the UHRFB collimator increased sphere detection compared with using the LEHR collimator, and that the LEHR collimator itself yielded better detection performance than the HRFB and LEUHR collimators. These observations held despite the large variability in detection performance between observers. This variability can be explained by the fact that although all observers were used to nuclear medicine image reading, they did not share the same level of expertise. Our results suggest that the choice of the collimator alters the detection performance regardless of the level of expertise of the observer.

Looking at the sensitivity of lesion detection for a similar specificity (about 60%) (table 8), the UHRFB increased the sensitivity by up to 20% (+10% for the I20 images, +19% for the I10 images and +6% for the I_{JAS} images). Although this increase varied with image type, the UHRFB collimator always yielded detection performances that were at least as good as and often better than those observed with the LEHR collimator for all image types. Such an increase in sensitivity would not be observed in clinical practice when changing from the LEHR collimator to the UHRFB collimator, since not all scans yield borderline images. However, for borderline images, our results suggest that there would be a worthwhile increase in sensitivity if the UHRFB collimator were used instead of the LEHR collimator. The other two collimators

Table 4. Areas under the ROC curves (AUC) ± standard error obtained for the I20 images.

Observer	LEHR	LEUHR	HRFB	UHRFB
1	0.74 ± 0.14	0.83 ± 0.12	0.46 ± 0.17	0.92 ± 0.08
2	0.75 ± 0.14	0.59 ± 0.17	0.50 ± 0.17	0.94 ± 0.07
3	0.84 ± 0.12	0.64 ± 0.16	0.67 ± 0.15	0.85 ± 0.11
4	0.53 ± 0.16	0.47 ± 0.17	0.70 ± 0.15	0.72 ± 0.15
5	0.85 ± 0.11	0.80 ± 0.14	0.74 ± 0.15	0.82 ± 0.12
6	0.79 ± 0.13	0.64 ± 0.16	0.93 ± 0.07	0.74 ± 0.15
7	0.66 ± 0.17	0.68 ± 0.16	0.67 ± 0.16	0.89 ± 0.09
8	0.85 ± 0.11	0.59 ± 0.17	0.47 ± 0.16	0.83 ± 0.12
9	0.83 ± 0.13	0.79 ± 0.13	0.80 ± 0.13	0.81 ± 0.12
10	0.67 ± 0.15	0.75 ± 0.15	0.50 ± 0.17	0.82 ± 0.12
Mean ± standard deviation	0.75 ± 0.10	0.68 ± 0.11	0.65 ± 0.16	0.84 ± 0.07

Table 5. Areas under the ROC curves (AUC) ± standard error obtained for the I10 images.

Observer	LEHR	LEUHR	HRFB	UHRFB
1	0.72 ± 0.15	0.75 ± 0.14	0.53 ± 0.17	0.90 ± 0.09
2	0.84 ± 0.12	0.61 ± 0.16	0.67 ± 0.16	0.94 ± 0.07
3	0.84 ± 0.13	0.49 ± 0.17	0.72 ± 0.17	0.85 ± 0.11
4	0.47 ± 0.18	0.45 ± 0.17	0.81 ± 0.13	0.80 ± 0.13
5	0.71 ± 0.16	0.65 ± 0.16	0.69 ± 0.16	0.90 ± 0.09
6	0.69 ± 0.15	0.62 ± 0.17	0.73 ± 0.15	0.79 ± 0.13
7	0.66 ± 0.16	0.72 ± 0.14	0.48 ± 0.17	0.89 ± 0.09
8	0.67 ± 0.15	0.79 ± 0.13	0.59 ± 0.20	0.95 ± 0.06
9	0.72 ± 0.15	0.59 ± 0.17	0.69 ± 0.15	0.98 ± 0.04
10	0.80 ± 0.13	0.82 ± 0.12	0.45 ± 0.17	0.89 ± 0.10
mean ± standard deviation	0.71 ± 0.11	0.65 ± 0.12	0.64 ± 0.12	0.89 ± 0.06

yielded sensitivity values that were about 10% lower than those of the LEHR collimator, for a similar specificity of 60%.

We tried to determine whether the different detection performances could be explained by the measured characteristics of the collimators. Comparing the collimator characteristics (table 3) and the ROC results (tables 4, 5, 6 and 7) showed that the physical characteristics of the collimators were not enough to predict their relative detection performances. Indeed, the performance in lesion detection depends on both spatial resolution and collimator sensitivity and probably also on other characteristics not so easy to identify (such as the magnification effect produced by fan-beam collimators). The good performance of the UHRFB collimator for the detection of the small spheres could be explained by its excellent spatial resolution (5.5 mm at 70 mm) at the distances considered in this work compared with those of the other three collimators (7.2 mm at 70 mm for the LEHR collimator). This high spatial resolution did not seem to be counterbalanced by the low sensitivity of the UHRFB collimator. Figure 3 shows the theoretical spatial resolution as a function of the source to collimator distance. This figure suggests that regarding spatial resolution, the benefit of using the UHRFB collimator instead of the LEHR collimator increases as the lesion becomes deeper, since the difference between the spatial resolution of the two collimators gets larger.

The respective performance of the LEHR and LEUHR collimators could be explained in terms of sensitivity: although the spatial resolution of the LEHR collimator was between 15% and 20% poorer than that of the LEUHR collimator at the distances of interest, the sensitivity of the LEHR collimator was 35% greater than that of the LEUHR collimator.

Table 6. Areas under the ROC curves (AUC) ± standard error obtained for the I_{JAS} images.

Observer	LEHR	LEUHR	HRFB	UHRFB
1	0.77 ± 0.13	0.76 ± 0.13	0.62 ± 0.15	0.81 ± 0.12
2	0.83 ± 0.12	0.54 ± 0.17	0.63 ± 0.15	0.84 ± 0.11
3	0.85 ± 0.13	0.79 ± 0.13	0.68 ± 0.15	0.84 ± 0.12
4	0.66 ± 0.16	0.58 ± 0.16	0.73 ± 0.15	0.73 ± 0.15
5	0.85 ± 0.11	0.75 ± 0.14	0.87 ± 0.09	0.80 ± 0.13
6	0.90 ± 0.88	0.59 ± 0.16	0.75 ± 0.13	0.82 ± 0.12
7	0.70 ± 0.17	0.61 ± 0.16	0.62 ± 0.16	0.82 ± 0.12
8	0.72 ± 0.14	0.64 ± 0.16	0.54 ± 0.16	0.81 ± 0.13
9	0.92 ± 0.07	0.71 ± 0.15	0.69 ± 0.15	0.85 ± 0.11
10	0.84 ± 0.11	0.60 ± 0.16	0.69 ± 0.14	0.88 ± 0.10
Mean ± standard deviation	0.80 ± 0.09	0.66 ± 0.09	0.68 ± 0.09	0.82 ± 0.04

Table 7. Results of multiple comparisons between collimators for the three types of images (I20, I10 and I_{JAS}). The name of the collimator yielding the best detection performance is shown in each cell, together with the corresponding p value of the Wilcoxon signed ranks test. — indicates that the two collimators were not found to yield significantly different performance.

Comparing	I20	I10	I_{JAS}
LEHR and LEUHR	—	—	LEHR, $p = 0.001$
LEHR and HRFB	—	—	LEHR, $p = 0.005$
LEHR and UHRFB	—	UHRFB, p=0.001	—
LEUHR and HRFB	—	—	—
LEUHR and UHRFB	UHRFB, $p = 0.001$	UHRFB, $p = 0.001$	UHRFB, $p = 0.001$
HRFB and UHRFB	UHRFB, $p = 0.008$	UHRFB, $p = 0.002$	UHRFB, $p = 0.007$

Table 8. Sensitivity/specificity trade-off (±1 standard deviation) averaged over the 10 observers for the four collimators and the three types of image (I20, I10 and I_{JAS}).

	Sensitivity/specificity		
	I20	I10	I_{JAS}
LEHR	$77.5 \pm 20.0/58.0 \pm 18.9$	$72.5 \pm 18.4/64.0 \pm 22.7$	$72.5 \pm 22.7/68.0 \pm 30.1$
LEUHR	$70.0 \pm 19.5/56.0 \pm 17.4$	$55.0 \pm 12.1/64.0 \pm 22.7$	$61.2 \pm 13.7/58.0 \pm 14.8$
HRFB	$62.5 \pm 20.1/50.0 \pm 18.4$	$60.0 \pm 21.9/65.0 \pm 26.9$	$63.7 \pm 23.9/63.3 \pm 18.9$
UHRFB	$87.5 \pm 12.5/68.0 \pm 28.6$	$91.3 \pm 8.4/64.0 \pm 22.7$	$78.7 \pm 8.7/70.0 \pm 21.6$

The difference in performance of the LEHR and HRFB collimators was more difficult to explain using the criteria of sensitivity and spatial resolution, since the HRFB collimator presented both a better spatial resolution (6.5 mm versus 7.2 mm at 70 mm) and a greater sensitivity (229 a.u. versus 188 a.u. at 70 mm) than the LEHR collimator. However, the count density in the images, which corresponds to the noise level, might explain the superiority of the LEHR collimator over the HRFB collimator. Indeed, with the HRFB collimator, there is a magnification effect in one direction which makes the physical pixel area smaller than with the LEHR collimator. Although the sensitivity of the HRFB collimator is larger than that of the LEHR collimator, the counts are distributed over a larger number of pixels for the HRFB collimator (as the pixel area is smaller), and the count density per pixel is therefore smaller, yielding a higher level of noise. The increased level of noise resulting from the use of a converging collimator has actually already been observed when comparing a pinhole collimator with a LEUHR collimator in planar imaging (Scarfone *et al* 1997). Such a noise increase also

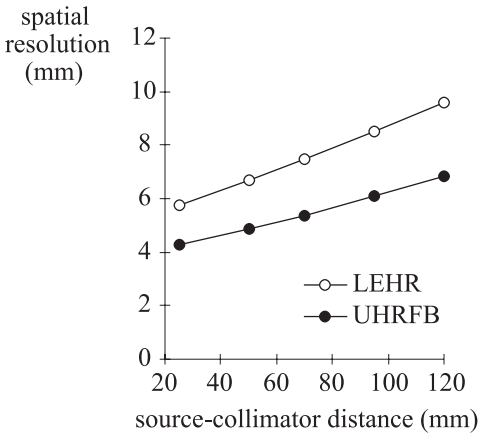

Figure 3. Spatial resolution as a function of the source–collimator distance for the LEHR and UHRFB collimators.

affected the UHRFB (table 3). However, in that case, the high spatial resolution seemed to provide a definite advantage in terms of lesion detection that was not counterbalanced by the increase in noise.

The fact that considerations regarding spatial resolution, sensitivity and noise level have to be invoked in turn to explain the respective performances of the collimators illustrates the difficulty of predicting the change in detection by considering only the physical characteristics of the collimator.

4.5. Effect of scatter correction

For each acquisition, we considered three types of image (I20, I10 and I_{JAS}) each corresponding to a different way of dealing with scatter, to determine whether the impact of the collimator depended on the type of image used in the clinical procedure. The choice of the collimator actually affected the detection performance similarly for all image types. This indicates that the *relative* performances of the collimators in a specific configuration were not greatly affected by the scatter contents of the images and suggests that the benefit of using the UHRFB collimator instead of the LEHR collimator might hold in configurations including thoracic and cardiac activities. Even if this was not the aim of this study, for each collimator we also compared the detection performance obtained with the different types of image. An image type effect was found only for the LEHR and UHRFB collimators. For the LEHR collimator, the I_{JAS} images yielded better detection than the I10 images (average AUC over the 10 observers were 0.805, 0.714 and 0.752 for the I_{JAS}, I10 and I20 images respectively). For the UHRFB collimator, the I10 images yielded better detection performance than either the I20 or the I_{JAS} images (average AUC over the 10 observers were 0.820, 0.888 and 0.835 for the I_{JAS}, I10 and I20 images respectively). These results are consistent with previously reported results (Buvat *et al* 1998) which demonstrated that I20 images yielded poorer detection performance than I10 or I_{JAS} images. In this previous study, however, no significant difference was found between I10 and I_{JAS} images. The fact that in the study reported here, I10 images yielded better sphere detection than I_{JAS} images for the UHRFB collimator but that the opposite was observed for the LEHR collimator might be explained by the difference in collimator sensitivities. Indeed, the UHRFB collimator presents a poorer sensitivity than the LEHR collimator (table 3), and

the noise increase resulting from count subtraction in the I_{JAS} images might cancel the benefit of scatter subtraction. Because of its higher sensitivity, this noise increase might not be such an issue with the LEHR collimator. In addition, the experimental configurations used in the study reported here do not correspond to the high scattering configurations used in the work of Buvat *et al* (1998). The effect of scatter correction was therefore expected to be small in the present study.

4.6. Study limitations

In this study spherical lesions were considered, but clinical lesions often have more complex shapes. Further investigations will have to be performed to determine whether the benefit of high spatial resolution reported in this study would be more or less important in detecting non-spherical clinical lesions.

5. Conclusion

Using a realistic breast phantom, we found that for borderline images the sensitivity of lesion detection was significantly affected by the choice of the collimator fitted to the gamma camera in planar SMM. For a similar specificity of about 60%, using a UHRFB collimator increased the sensitivity by up to 20%. The detection performances observed with the UHRFB collimator were at least as good as and often better than those observed with the LEHR collimator for images acquired in a 10% energy window as well as for images acquired in a 20% energy window or corrected for scatter using the Jasczczak subtraction. This suggests that in conventional planar SMM, using a UHRFB collimator instead of the commonly used LEHR collimator could significantly improve the detection sensitivity of lesions that are less than 15 mm in diameter and that present low lesion-to-background activity ratios (from 2 to 5), without adversely affecting the detection specificity. Complementary clinical studies should be performed to determine whether changing the LEHR collimator for a UHRFB collimator in planar SMM might be a convenient way to improve sensitivity for detection of small lesions while awaiting the wider availability of dedicated nuclear mammographs.

Acknowledgments

The authors thank A M Bernard, M C De Sousa, M Di Paola, A Devillers, M G Dondon, E Garin, S Girault, M L Ménot and M Pélégrini for the time they spent on this work.

References

Buvat I, De Sousa M C, Di Paola M, Ricard M, Lumbroso J and Aubert B 1998 Impact of scatter correction in planar scintimammography *J. Nucl. Med.* **39** 1590–6

Dorfman D D and Alf E 1969 Maximum likelihood estimation of parameters of signal detection theory and determination of confidence intervals—rating-method data *J. Math. Psych.* **6** 487–96

Hanley J A and McNeil B J 1982 The meaning and use of the area under the receiver operating characteristic (ROC) curve *Radiology* **143** 29–36

Jaszczak R J, Floyd C E and Coleman R E 1985 Scatter compensation techniques for SPECT *IEEE Trans. Nucl. Sci.* **32** 786–93

Khalkhali I, Diggles L E, Taillefer R, Vandestreek P R, Peller P J and Abdel-Nabi H H 1999 Procedure guideline for breast scintigraphy *J. Nucl. Med.* **40** 1233–5

Khalkhali I, Mena I, Jouanne E, Diggles L, Venegas R, Block J, Alle K and Klein S 1994 Prone scintimammography in patients with suspicion of carcinoma of the breast *J. Am. Coll. Surg.* **178** 491–7

Maini C L, de Notaristefani F, Tofani A, Iacopi F, Sciuto R, Semprebene A, Malatesta T, Vittori F, Frezza F, Botti C, Giunta S and Natali P G 1999 99mTc-MIBI scintimammography using a dedicated nuclear mammograph *J. Nucl. Med.* **40** 46–51

Maublant J, de Latour M, Mestas D, Clemenson A, Charrier S, Feiffel V, Le Bouedec G, Kaufmann P, Dauplat J and Veyre A 1996 Technetium-99m-sestamibi uptake in breast tumor and associated lymph nodes *J. Nucl. Med.* **37** 922–5

Mekhmandarov S, Sandbank J, Cohen M, Lelcuk S and Lubin E J 1998 Technetium-99m-MIBI scintimammography in palpable and nonpalpable breast lesions *J. Nucl. Med.* **39** 86–91

Metz C E 1986 Basic principles of ROC analysis *Semin. Nucl. Med.* **8** 283–98

Moore S C, Kouris K and Cullum I 1992 Collimator design for single photon emission tomography *Eur. J. Nucl. Med.* **19** 138–50

Palmedo H, Schomburg A, Grünwald F, Mallmann P, Krebs D and Biersack H J 1996 Scintimammography with Tc-99m MIBI in suspicious breast lesions *J. Nucl. Med.* **37** 626–30

Scarfone C, Jaszczak R J, Li J, Soo M S, Smith M F, Greer K L and Coleman R E 1997 Breast tumor detection using incomplete circular orbit pinhole SPET: a phantom study *Nucl. Med. Comm.* **18** 1077–86

Scopinaro F, Mezi S, Ierardi M, De Vincentis G, Tiberio N S, David V, Maggi S, Sallusti E and Modesti M 1998 ^{99m}Tc MIBI prone scintimammography in patients with suspicious breast cancer: relationship with mammography and tumor size *Int. J. Oncol.* **12** 661–4

Scopinaro F, Pani R, De Vincentis G, Soluri A, Pellegrini R and Porfiri L M 1999 High-resolution scintimammography improves the accuracy of technetium-99m methoxyisobutylisonitrile scintimammography: use of a new dedicated gamma camera *Eur. J. Nucl. Med.* **26** 1279–88

Siegel S and Castellan N J 1988 *Nonparametric Statistics for the Behavioral Sciences* (New York: McGraw-Hill)

Taillefer R 1999 The role of 99mTc-sestamibi and other conventional radiopharmaceuticals in breast cancer diagnosis *Semin. Nucl. Med.* **29** 16–40

Tsui B M W, Wessel D E, Zhao X D, Wang W T, Lewis D P and Frey E C 1998 Imaging characteristics of scintimammography using parallel-hole and pinhole collimators *IEEE Trans. Nucl. Sci.* **45** 2155–61